Geophysical Research Letters

Plant Water Uptake Thresholds Inferred From Satellite Soil Moisture

Maoya Bassiouni[1,2] (ID), **Stephen P. Good**[1] (ID), **Christopher J. Still**[3] (ID), **and Chad W. Higgins**[1]

[1]Department of Biological and Ecological Engineering, Oregon State University, Corvallis, OR, USA, [2]Department of Crop Production Ecology, Swedish University of Agricultural Sciences, Uppsala, Sweden, [3]Department of Forest Ecosystems and Society, Oregon State University, Corvallis, OR, USA

Abstract Empirical functions are widely used in hydrological, agricultural, and Earth system models to parameterize plant water uptake. We infer soil water potentials at which uptake is downregulated from its well-watered rate and at which uptake ceases, in biomes with <60% woody vegetation at 36-km grid resolution. We estimate thresholds through Bayesian inference using a stochastic soil water balance framework to construct theoretical soil moisture probability distributions consistent with empirical distributions derived from satellite soil moisture observations. The global median Nash–Sutcliffe efficiency between empirical soil moisture distributions and theoretical distributions using reference constants, inferred median parameters per biome, and spatially variable inferred parameters are 0.38, 0.59, and 0.8, respectively. Spatially variable thresholds capture location-specific vegetation and climate characteristics and can be connected to biome-level water uptake strategies. Results demonstrate that satellite soil moisture probability distributions encode information, valuable to understanding biome-level ecohydrological adaptation and resistance to climate variability.

Plain Language Summary Vegetation regulates a large fraction of the terrestrial water and carbon cycles as it adapts and responds to changing environmental conditions such as soil moisture availability, yet our ability to characterize diversity in vegetation soil water-use behavior at large scales is limited. In this study, we analyze satellite observations to estimate thresholds that are commonly used to approximate when vegetation extracts water from the soil. We show that the newly found values are more consistent with global patterns of soil moisture compared to constants found in the literature. Spatially variable plant water uptake thresholds reflect land cover and climate characteristics and can be connected to water-use strategies in biomes not dominated by trees.

1. Introduction

Transpiration accounts for over 50% of the global transfer of water from the land back to the atmosphere (Good et al., 2015). Vegetation regulates terrestrial water and carbon cycles as it responds and adapts to changing environmental conditions such as soil moisture availability. The driving force moving water from soils, through plant tissue, and to the atmosphere is the gradient in potential energy state of water (Tyree, 2003). Thus, soil water potential strongly controls transpiration. Plant water uptake is conceptually bound between thresholds when stomata are fully open, before which plant water uptake is maximum, and when stomata are fully closed, after which plant water uptake ceases. Plant water uptake thresholds have been incorporated into soil water-limitation constraints on evaporation (Feddes et al., 1976), often termed β functions, and are used in many hydrological (Laio et al., 2001; Westenbroek et al., 2018), agricultural (Hlavinka et al., 2011; Steduto et al., 2009), and Earth system (Baker et al., 2008; Clark et al., 2011; Niu et al., 2011; Oleson et al., 2013) models.

Contemporary applications routinely parameterize plant water uptake thresholds using universal constants because spatially variable values, which account for diversity of plant responses to environmental stress, are generally unavailable. For example, the threshold at which plant water uptake ceases, historically termed the "wilting point" (Briggs & Shantz, 1912), is commonly set to −1.5 MPa. This value was determined experimentally (Richards & Weaver, 1944) based on observations of leaf vigor in herbaceous plants; however, visible plant phenological change, such as wilting, may not coincide with the threshold when roots stop

extracting soil water. Hydrologically meaningful thresholds need to be determined through a framework reflective of soil water balance.

Empirical soil water-limitation functions, parameterized with reference constants in many biosphere models, are generally unable to realistically represent effects of soil moisture on stomatal conductance (Fatichi et al., 2016; Powell et al., 2013). Furthermore, soil moisture-limited productivity represents a large and uncertain component of the simulated terrestrial carbon cycle (Trugman et al., 2018). Recent efforts show that water uptake thresholds drive sensitivity of flux estimates in Earth system models (Arsenault et al., 2018) and calibrating wilting points to be consistent with observed spatial patterns in soil moisture improves simulations (Qiu et al., 2018).

Plant resilience and response to environmental stress is governed by complex and diverse plant hydraulic traits (Anderegg et al., 2016; Skelton et al., 2015), which are expected to vary depending on vegetation type, hydroclimatic conditions, ecosystem diversity, and scale. Plant hydraulic strategies vary along a continuum from drought avoidant to drought tolerant, coupled with safety margins that vary from conservative to risky (Skelton et al., 2015). Drought-avoidant plants favor water conservation, with strict stomatal closure in response to drying soils, and can be associated with isohydry. Drought-tolerant plants favor carbon assimilation, maintain high stomatal conductance even as soils dry, risking damage due to embolism, and can be associated with anisohydry (Meinzer et al., 2016). The overall relation between stomatal control and soil moisture may be strongly related to climate aridity because many traits are coordinated and reflect trade-offs between water conservation and plant growth (Li et al., 2018).

Water and carbon fluxes are sensitive to diversity of plant traits within an ecosystem, and the efficacy of summarizing these complex interactions with a single value, resulting from coexistence of species, is uncertain (Pappas et al., 2016). Remotely sensed observations have been used to identify broad spatial patterns of plant hydraulic behavior and water-limitation response beyond the species level and across biogeographic regions (Feldman et al., 2018; Konings & Gentine, 2017). Global surface soil moisture observations, available through National Aeronautics and Space Administration's Soil Moisture Active Passive (SMAP) mission (Chan et al., 2016; Entekhabi et al., 2010), offer opportunities to diagnose satellite-scale soil water balance (Akbar et al., 2019; McColl et al., 2017) and are statistically coupled with ecosystem-relevant subsurface moisture (Short Gianotti et al., 2019). Relating large-scale canopy and soil water dynamics remains challenging because vegetation response to water available in soil layers that are deeper than those sensed by satellites is uncertain (Feldman et al., 2018). Efforts focused on canopy water content do not directly translate dynamics of water uptake, necessary to model the water balance.

We address the need to gain a broader spatial understanding of plant water uptake thresholds and estimate hydrologically meaningful values at the ecosystem scale. Our approach is independent of vegetation data, does not require rooting zone soil moisture measurements, and uses shallow satellite soil moisture sensing depth to its advantage. The shape of local soil moisture probability distributions ($p(s)$) are constrained by water uptake thresholds according to a commonly used stochastic soil water balance framework (Laio et al., 2001). A parsimonious theoretical model of $p(s)$ can be inverted using the Bayes theorem to estimate ecohydrological parameters (Bassiouni et al., 2018).

This simple modeling framework does not account for the full complexity of stomatal control; however, ecohydrological parameters that constrain $p(s)$ can be analytically related to plant hydraulic traits and water-use strategies (Manzoni et al., 2014). Empirical $p(s)$ derived from satellite observations and ground-based measurements are not necessarily comparable because processes controlling the soil moisture dynamics are different at each scale and require scale-specific parameters (Bassiouni et al., 2018). Plant water uptake thresholds consistent with large-scale $p(s)$, which capture the integrated dynamics of grid-specific vegetation and climate, may enable more realistic application of widely used empirical soil water-limitation functions.

We test the hypothesis that satellite soil moisture encodes plant water uptake strategies and we can extract this information through inverse modeling. The focus of this study is to determine values of ecohydrological parameters that best fit empirical $p(s)$ derived from satellite soil moisture. We estimate plant water uptake thresholds that are relevant to β-type soil water-limitation functions commonly used to constrain evapotranspiration. We describe variability in ecohydrological parameters by vegetation type and climate aridity. Finally, we summarize trends in inferred ecohydrological patterns and evaluate their connection to biome-level water uptake strategies.

2. Data

We conduct all analysis at a spatial resolution of 36 km EASE-Grid 2.0 with data spanning April 2015 to March 2019. The first three-year period is used for parameter estimation and the fourth year for validation. Soil moisture at about 5 cm depth is obtained from daily 36 km SMAP L3 (Version 5) (O'Neill et al., 2018). We analyzed only soil moisture estimates flagged as recommended by the data product, that is, those unaffected by water bodies, dense vegetation, frozen soil, and radio frequency interference. This restricts our analysis to temperate and tropical biomes with <60% woody vegetation, representing approximately half of the global land surface. We compute, for each grid cell, from 3-hourly 9 km SMAP L4 (Version 4) geophysical data (Reichle et al., 2018) average daily rainfall depth and frequency (α and λ, Rodriguez-Iturbe et al., 1984), average daily rate of equilibrium evaporation (E_p, Priestley & Taylor, 1972) over estimation and validation periods, and the aridity index (AI), defined as the ratio of total annual precipitation to E_p, over the 4-year record. Soil hydraulic parameters at 5 cm depth are available at a spatial resolution of 0.25° (Montzka et al., 2017) and are regridded to 36 km EASE-Grid 2.0. The biome of each grid cell is classified with the International Geosphere-Biosphere Programme (IGBP) (Kim, 2013). We separate grasslands into two classes: temperate, above 35° north/south latitude and typically dominated by C3 grasses; and tropical/subtropical, from the equator to 35° north/south latitude and typically dominated by C4 grasses (Still et al., 2003).

3. Methods

3.1. Definition of Ecohydrological Parameters

We estimate four ecohydrological parameters of a piecewise soil moisture loss function (Laio et al., 2001, Figure S1 in the supporting information) for each grid cell with at least 365 daily SMAP soil moisture over the 3-year estimation period: soil saturation at incipient stomatal closure (s^*), soil saturation at full stomatal closure (s_w), relative rate of evapotranspiration losses from the surface soil under well-watered conditions ($E_{\max}/E_p$), and relative rate of surface soil water losses at the point of full stomatal closure (E_w/E_p).

We convert s^* to Ψ^*, soil water potential at which evapotranspiration losses from the surface soil are down-regulated from their maximum well-watered rate, and s_w to Ψ_0, soil water potential at which plant water uptake from the surface soil ceases, using the Mulalem-van Genuchten equation (Montzka et al., 2017). Thresholds Ψ^* and Ψ_0 thus provide more universal measures to compare plant water uptake behavior across locations. The ratio of evapotranspiration losses from the surface soil under well-watered conditions to equilibrium evaporation ($E_{\max}/E_p$) is related to the surface-atmosphere decoupling coefficient (Jarvis & McNaughton, 1986; Peng et al., 2019).

3.2. Inference of Ecohydrological Parameters

We consider, for each grid cell, a daily water balance (Text S1a) forced with stochastic rainfall inputs (α, λ derived from data), for a 5 cm soil column (approximate SMAP sensing depth) with known soil physical characteristics (Montzka et al., 2017). Under the assumption of steady state, locations with the same climate and soil but different plant water uptake thresholds have different theoretical $p(s)$ (equation S1, Laio et al., 2001).

The stochastic soil water balance framework is particularly compatible with Bayesian inference because it provides an analytical equation for a likelihood function (equation S3). We use the Bayes theorem to relate theoretical $p(s)$ to empirical $p(s)$, derived from satellite soil moisture and estimate ecohydrological parameters using a Metropolis-Hastings Markov chain Monte Carlo algorithm (Bassiouni et al., 2018). We repeat the algorithm three times with 20,000 steps (10,000 step burn-in period) and determine that parameters have converged when each Gelman-Rubin diagnostic is below to 1.1 (Bloom & Williams, 2015; Gelman & Rubin, 1992).

Bayesian inference provides means to evaluate when information is insufficient to estimate ecohydrological parameters. High goodness-of-fit between theoretical and empirical $p(s)$ does not directly imply that inferred parameters translate realistic plant water uptake behavior. We use the coefficient of variation of posterior parameter estimates to measure uncertainty. We discard nonconverging results to reduce some, but not all, concerns of equifinality.

We calculate a theoretical best fit $p(s)$ using mean values of posterior parameter estimates and a reference $p(s)$ using constants ($\Psi_0 = -1.5$ MPa; $\Psi^* = -0.033$ MPa; $E_{max}/E_p = 1$; $E_w/E_p = 0$). We evaluate goodness-of-fit for the validation period between empirical $p(s)$ derived from satellite soil moisture and both best fit and reference theoretical $p(s)$ using a quantile-level Nash-Sutcliffe efficiency (NSE) (Müller et al., 2014).

3.3. Limitations

Our approach based on steady state statistical properties of hydrologic and climatic variables overcomes certain limitations of large-scale analyses to detect ecosystem-scale patterns; however, inferred parameters are associated with surface soil dynamics and may not represent the full complexity of stomatal control for an entire plant.

The inverse modeling framework can provide hydrologically meaningful plant water uptake thresholds, because it parameterizes the water balance of the soil column depth at which satellite soil moisture is observed. We also expect to detect plant water uptake thresholds, which are better constrained, because soil moisture in the shallow surface soil column is more homogenous in depth than soil moisture integrated over a deeper rooting zone.

The shallow satellite soil moisture sensing depth also benefits the inverse modeling approach because soil moisture is more dynamic at the surface compared to soil moisture integrated over the active rooting depth. Satellite soil moisture observations thus span a larger range of wet to dry values necessary to construct empirical $p(s)$. The probabilistic framework also overcomes some limitations of process-based models and satellite-scale data because it does not require concurrent time series of hydroclimatic variables, is not affected by gaps in observations, relies on few parameters, (Bassiouni et al., 2018), and has relatively low computational cost.

Our model does not partition plant transpiration and soil water evaporation losses from the surface soil, and this is a challenge in most ecohydrological studies (Stoy et al., 2019). We can assume Ψ_0, Ψ^*, and E_{max}/E_p generally reflect plant water uptake behavior if the shape of the piecewise function for soil water losses (Figure S1) is determined by vegetation. This may not be true in all locations, particularly where evaporation dominates surface soil water losses compared to transpiration. Barren landscapes, which have less than 10% vegetation cover, provide estimates of baseline soil water loss functions dominated by soil water evaporation and help compare soil versus plant controls on the shape of the piecewise function.

We provide additional discussion on method assumptions and limitations and define the equation for $p(s)$ and all model parameters in Text S1. All parameter values for $p(s)$ and inverse modeling diagnostics (convergence, uncertainty, goodness-of-fit) are reported in a global data set (Bassiouni, 2020a). Scripts associated with this analysis are publicly available (Bassiouni, 2018, 2020b).

3.4. Evaluation of Ecohydrological Patterns

We hypothesize that combinations of inferred ecohydrological parameters produce diverse water uptake strategies encoded in SMAP. We thus need to evaluate how ecohydrological parameters, inferred independently of vegetation data and rooting zone moisture, relate to existing knowledge of plant water uptake behavior.

Plants make trade-offs between carbon assimilation and water conservation (e.g., Skelton et al., 2015) and need to balance plant water uptake and stress from water loss. We combine these contrasting dynamics in a soil water loss index (ε, equation S4), that is normalized by precipitation and weighted by stress (Manfreda et al., 2017; Porporato et al., 2001). We derive biome-level ecohydrological trends to evaluate and interpret plant water uptake patterns encoded in SMAP data. We connect these trends to drought-avoidant and drought-tolerant water uptake behaviors, with respect to the inferred parameters.

We calculate the sensitivity of the absolute value of ecohydrological parameters ($X = |\Psi_0|, |\Psi_1|, E_{max}/E_p$) to AI to quantify ecohydrological adaptation ($\partial X/\partial AI$) and the sensitivity of ε to AI to quantify ecohydrological resistance ($\partial \varepsilon/\partial AI$) for each IGBP class with the nonparametric Thiel-Sen estimator (Theil, 1992, Text S3). Positive ecohydrological adaptation translates to a more drought-tolerant strategy with respect to a parameter with greater aridity. Positive ecohydrological resistance translates to a relative increase in water uptake, given the combination of ecohydrological parameters, as conditions become less favorable.

4. Results and Discussion

4.1. Estimates of Ecohydrological Parameters

Inferred parameters Ψ_0, Ψ^*, and E_{max}/E_p construct theoretical descriptions of $p(s)$ that are consistent with empirical $p(s)$ derived from satellite soil moisture, and parameters are highly variable spatially (Figures 1a–1d). The calibrated stochastic soil water balance framework, although based on a very simplified piecewise function of soil water losses, performs well in many locations worldwide, and overall parameters inferred from satellite soil moisture are well constrained. We thus explore whether patterns of mean values of posterior parameter estimates for each grid cell reflect diversity in biome-level water uptake strategies and how they relate to vegetation type and climate.

Global median NSE between empirical and best fit theoretical $p(s)$ for the validation period is 0.80. Only locations for which NSE > 0.5 are included in subsequent analyses. The coefficient of variation of posterior parameter estimates is a measure of uncertainty we derive from the Bayesian model inversion, and median coefficients of variation are 2%, 5%, 7%, and 9% for s_w, s^*, E_{max}/E_p, and E_w/E_p, respectively. Ecohydrological parameters for the most humid and most arid locations either do not converge or provide poor validation (Figure 1d). Soil moisture observations at these locations do not span a large enough range of values between soil saturation and residual soil moisture to construct empirical $p(s)$, and our inference method is thus not effective. Global median NSE between empirical and reference theoretical $p(s)$ is 0.38, and goodness-of-fit is generally inferior to best fit theoretical $p(s)$ (Figure 1e). Reference constants did not accurately characterize $p(s)$ in many of the most arid regions of the world and best characterized $p(s)$ in North American grasslands and European croplands.

Thresholds estimated here are associated with stomatal control only in so far as they influence water uptake from the ~ 5 cm soil column considered and may not translate the physiological behavior of the entire plant, which can also extract water from deeper layers (Text S1e). Whole-plant transpiration is expected to stop when all soil layers in the rooting zone have dried past the critical soil water potential and plant water storage (capacitance) is exhausted. By the time deeper soil layers have dried past plant water uptake thresholds, surface soil, sensed by satellites, is generally much drier, and concurrent surface soil water potential would be more negative than plant water uptake thresholds. This could be a reason why the canonical wilting point value of −1.5 MPa, which is based on plant vigor, when whole-plant transpiration ceases, is more negative than our inferred Ψ_0 values, based only on the surface soil water balance. Prior satellite estimates of thresholds at which vegetation water content decreases correspond to more negative soil water potentials than those found in this study (Feldman et al., 2018). Models that represent water uptake from different soil layers typically use same thresholds for each depth (Baker et al., 2008; Clark et al., 2011; Oleson et al., 2013). It is unknown whether root tissues stop uptake in their respective layers at similar soil water potentials and if our inferred Ψ_0 and Ψ^* thresholds can be applied to model soil water balance in other layers of the rooting zone.

4.2. Variability in Ecohydrological Parameters by Vegetation Type

We summarize ecohydrological parameters using IGBP classifications to explore variability in water uptake strategies by biome (Figures 2a–2c). Global median NSE between empirical and best fit theoretical $p(s)$ using median inferred parameters for each biome is 0.59. Median ecohydrological parameters for each biome inferred from satellite soil moisture (Table S1) may therefore be an improvement over reference constants, although parameter variability within each biome is large and only a small portion of this variability is explained by AI (Table S2).

Median Ψ_0 is most negative for both temperate and tropical/subtropical grasslands and least negative for woody savannas and savannas (Figure 2a). Grasslands can extract water from drier soils than other biomes. This implies that grasslands have more drought-tolerant strategies, with respect to Ψ_0, while woody savannas and savannas have more drought-avoidant strategies.

Median Ψ^* is similar for all biomes. It is most negative for temperate grasslands and least negative for croplands and tropical/subtropical grasslands. (Figure 2b). Temperate grasslands can withdraw soil water at a maximum rate from drier soils than other biomes. This implies that temperate grasslands, typically dominated by C3 grasses, have generally more drought-tolerant strategies, with respect to Ψ^*, compared to tropical/subtropical grasslands, typically dominated by C4 grasses and croplands, which often need irrigation in temperate regions to sustain optimal growth.
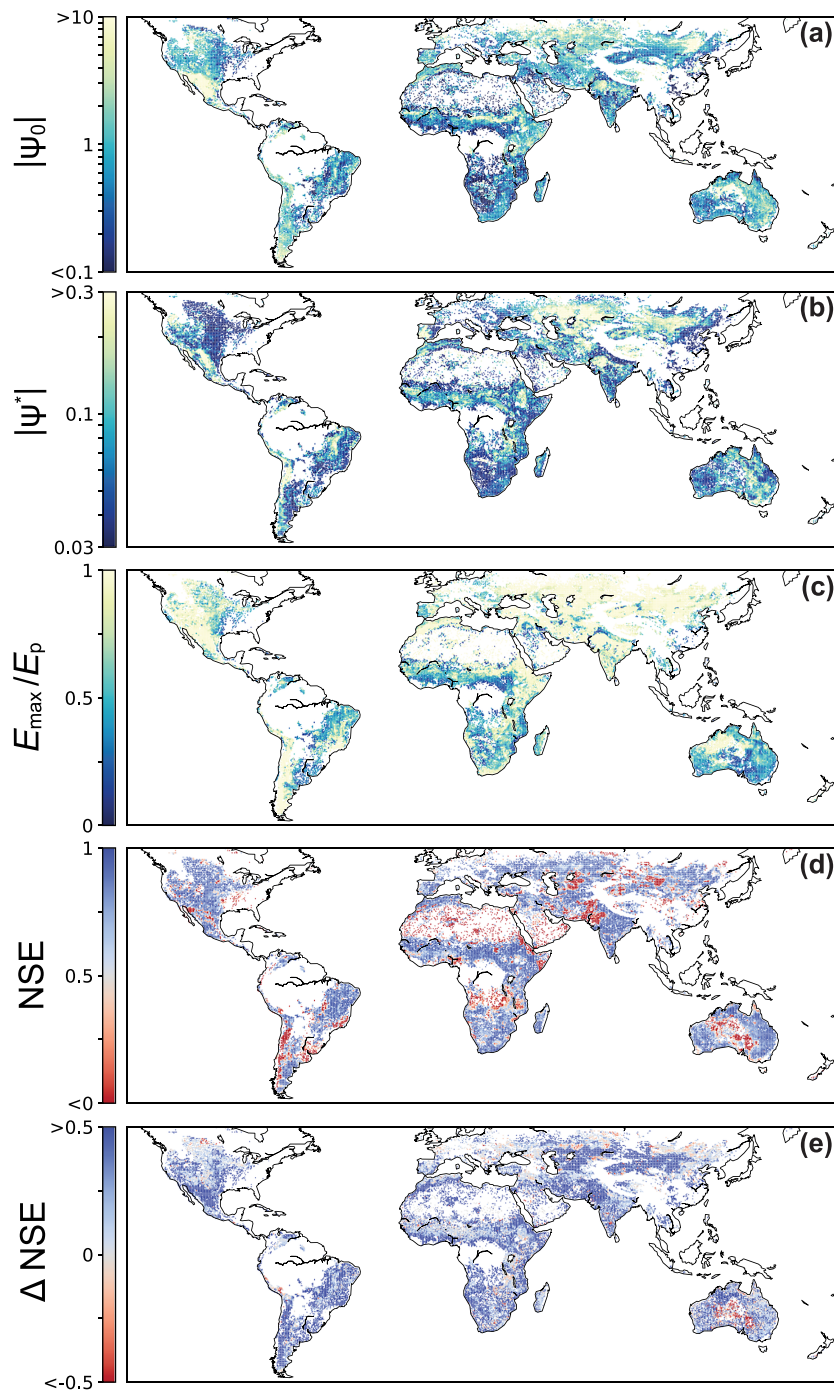
Figure 1. Ecohydrological parameters, which best fit empirical $p(s)$ derived from satellite observations. (a) $|\Psi_0|$, soil water potential when plant water uptake from the surface soil ceases, MPa. (b) $|\Psi^*|$, soil water potential when evapotranspiration losses from the surface soil are downregulated from their maximum rate, MPa. (c) E_{max}/E_p, normalized maximum rate of evapotranspiration losses from the surface soil. (d) NSE, goodness-of-fit between best fit theoretical versus empirical $p(s)$. (e) Difference in NSE between best fit and reference theoretical $p(s)$. Mean values of posterior parameter estimates are visualized. Locations with insufficient observations or nonconverging results are white.

Median E_{max}/E_p is close to 1 for temperate grasslands and about 0.5 for savannas and woody savannas (Figure 2c). Evapotranspiration is generally more coupled with radiation-limited equilibrium evaporation in aerodynamically smooth systems such as grasslands, whereas evapotranspiration is more coupled with stomatal conductance in aerodynamically rougher systems such as woody savannas (Jarvis & McNaughton, 1986; Peng et al., 2019).

Temperate grasslands are the biome for which median inferred parameters are closest to reference constants, which are based on observations made in temperate climates (Richards & Weaver, 1944). Savannas and woody savannas are abundant in tropical hot environments, and most often these are semiarid or seasonally dry locations. Leaf-to-air vapor pressure gradient may be much larger in savannas, woody savannas, and tropical/subtropical grasslands than in temperate grasslands, although Ψ_0 and Ψ^* are more negative in temperate grasslands.

Soil water losses for barren landscapes are primarily due to soil water evaporation and effects of downregulation from sparse vegetation may be minimal. Results for barren landscapes compared to other biomes are generally consistent with our expectation for soil water evaporation (Or et al., 2013). Median ecohydrological parameters for barren landscapes indicate that soil water evaporation becomes water limited at a less negative soil water potential than when transpiration becomes water limited; and maximum soil water losses are close to equilibrium evaporation. We can thus assume that variability in inferred ecohydrological parameters between biomes is mainly controlled by vegetation, although it is uncertain to what extent soil water evaporation affects local parameters.

4.3. Relation Between Ecohydrological Parameters and Aridity

Variability of ecohydrological parameters within each biome may reflect responses or adaptations to local environmental conditions. Stomatal conductance generally decreases exponentially with increasing vapor pressure deficit (Oren et al., 1999), and actual evapotranspiration may be downregulated from its potential value even when soil moisture is not limited (Novick et al., 2016). Trends between ecohydrological parameters and AI are evaluated for each biome using a 95% significance level (Table S2).

Trends between $|\Psi_0|$ and AI are positive for woody savannas and crop and natural vegetation mosaic; negative for croplands, open shrublands, and temperate grasslands; about null for savannas and tropical/subtropical grasslands; and overall strongest for woody savannas (Figure 2d and Table S2). Woody savannas and crop and natural vegetation mosaic can extract water from drier soils as climate conditions become more arid. This implies that water uptake strategies, with respect to Ψ_0, tend to be more drought tolerant as aridity increases in biomes with some trees; tend to be more drought avoidant as aridity increases in biomes dominated by shrubs or C3 grasses; and do not adapt for tropical/subtropical grasslands and savannas, dominated by C4 grasses.

Trends between $|\Psi^*|$ and AI are positive for open shrublands and croplands; negative for savannas, woody savannas, and tropical/subtropical grasslands; about null for crop and natural vegetation mosaic, and temperate grasslands; and overall strongest for savannas (Figure 2e and Table S2). Open shrublands and croplands can extract water at a maximum rate from drier soils as climate conditions become more arid, while savannas and tropical/subtropical grasslands downregulate water uptake at wetter thresholds. This implies that water uptake strategies, with respect to Ψ^*, tend to be more drought avoidant as aridity increases, for biomes dominated by C4 grasses, and tend to be more drought tolerant for open shrublands and croplands. Such patterns are consistent with anisohydric behavior, which is more common in arid shrublands and croplands (Fu & Meinzer, 2019; Konings & Gentine, 2017).

Trends between E_{max}/E_p and AI are negative for open shrublands, croplands, and crop and natural vegetation mosaic and strongest for open shrublands (Figure 2f and Table S2). When conditions are energy limited ($AI < 1.5$), E_{max}/E_p tends to increase with aridity for woody savannas and then decrease in water-limited conditions ($AI > 1.5$). There is no trend between E_{max}/E_p and AI for both temperate and tropical/subtropical grasslands and savannas, and reflect behavior of aerodynamically uncoupled land covers (Jarvis & McNaughton, 1986).

Trends between ecohydrological parameters ($|\Psi^*|$ and E_{max}/E_p) and AI for barren landscapes are null. This is consistent with our expectation that AI does not affect the shape of the soil water loss function dominated by soil water evaporation.
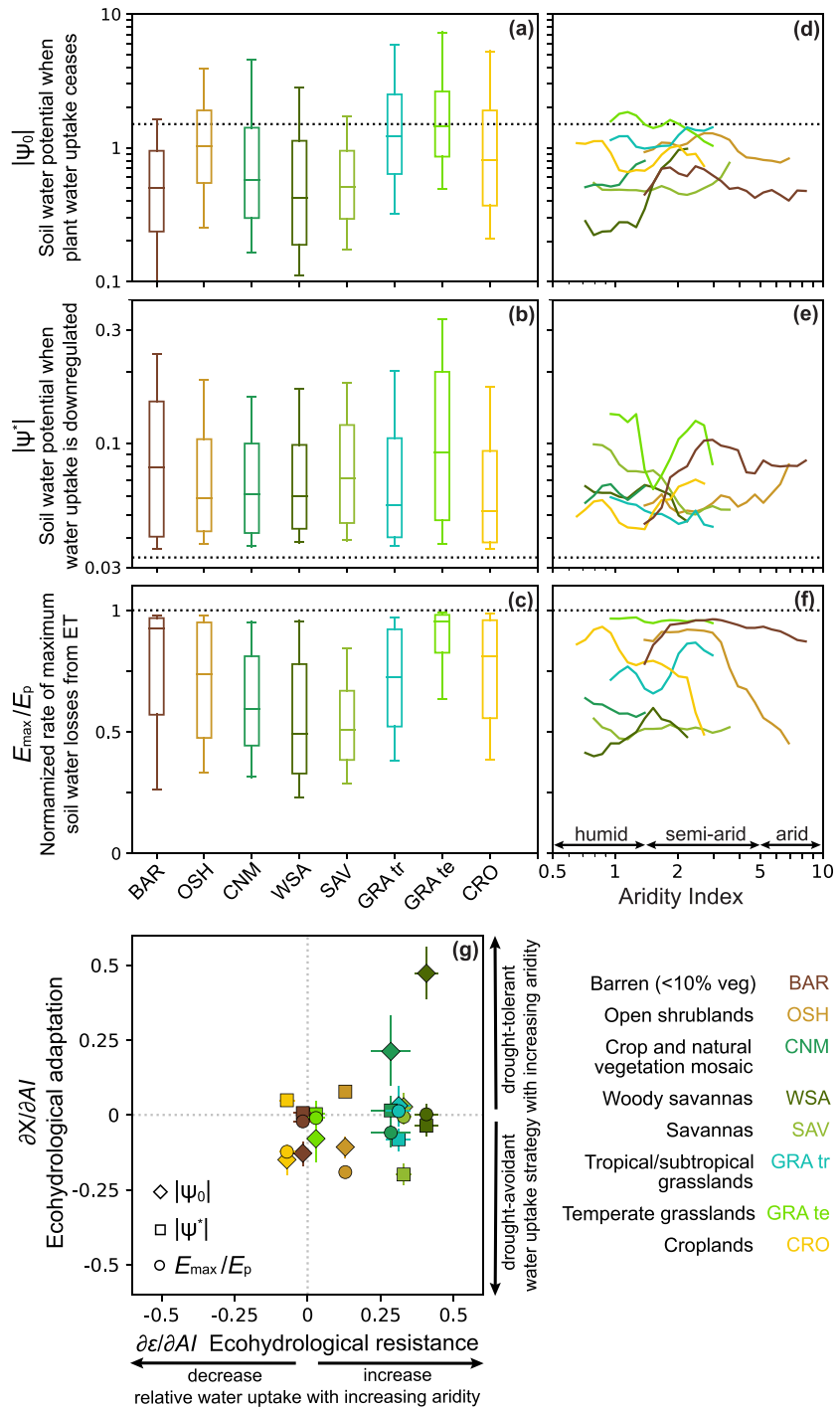
Figure 2. Biome-level ecohydrological trends. (a–c) Ecohydrological parameter variability by biome. Interquartile range (boxes), median (horizontal lines), 10th and 90th percentiles (whiskers), reference constants (dotted lines), values and sample sizes (Table S1). (d–f) Median biome ecohydrological parameters by aridity index bins. (g) Ecohydrological adaptation versus resistance, 95% confidence intervals (vertical and horizontal lines over markers), values and significance (Table S2).

4.4. Connection to Biome-Level Water Uptake Strategies

Geographic distribution of plant species is largely driven by vegetation sensitivity to drought (Engelbrecht et al., 2007). Theory suggests that plants become more efficient as water becomes scarce (Troch et al., 2009). Plant species with trait plasticity produce phenotypes adapted outside their optimal environments (Sultan, 2000) and can withstand a larger range of climates, but sometimes also trade-off overall lowers efficiency compared to specialized plants in their optimal climate.

We relate ecohydrological adaptation with ecohydrological resistance to connect inferred plant water uptake thresholds to biome-level water uptake strategies (Figure 2g). Our results only reflect drought-tolerant and drought-avoidant strategies with respect to the relation between water uptake and soil moisture at the surface. Our results are not able to provide direct information about total plant water uptake and do not necessarily reflect the overall drought survival of a biome. For example, extraction of groundwater using deep roots is globally prevalent (Evaristo & McDonnell, 2017).

Woody savannas, savannas, and tropical/subtropical grasslands have the most resistant water uptake strategies of the biomes we analyzed. Woody savannas and savannas may be more effective at extracting soil water in arid conditions compared to other biomes because the combination of individual ecohydrological parameter adaptations with AI results in an overall expansion of plant capacity to uptake water. In addition, C4 grasses, which often occur in hot, water-limited environments, tend to have higher water-use efficiency compared to other plant functional types (Still et al., 2003). Ecohydrological parameters associated with temperate grasslands dominated by C3 grasses are less variable with climate, and temperate grasslands are overall less resistant compared to woody savannas and savannas. Plant species, which are specialized at using resources in a particular climate, can experience greater stress in climatic conditions outside their optimal range (Sultan, 2000). Ecohydrological resistance is negative for croplands, suggesting water uptake strategies that do not withstand increasingly arid conditions and compromise their capacity to uptake water. Ecohydrological resistance is close to zero for barren landscapes.

Our results indicate that water uptake strategies in arid locations are generally more drought resistant. This is consistent with species-level studies of plant isohydricity (Fu & Meinzer, 2019; Li et al., 2018), although this trend is more uncertain in previous global studies (Konings & Gentine, 2017). Our results indicate that ecohydrological parameters for biomes with the highest ecohydrological resistance adapt to exploit water from low soil moisture states, occurring more frequently in arid conditions. In contrast, biomes with the lowest ecohydrological resistance are less able to exploit soil water during the more frequent low soil moisture states, because as climate becomes more arid, stomatal closure tends to be delayed toward drier conditions to use soil water at a maximum rate longer, while ceasing plant water uptake at a wetter threshold. Ecosystems with high ecohydrological resistance, with respect to our results, may be saving water when it is more available for later opportunities, while ecosystems with low ecohydrological resistance take up water with a more instantaneous gain. These patterns are relevant to understanding optimal stomatal conductance theories at different temporal and spatial scales (Mencuccini et al., 2019).

We compare vegetation water-use sensitivity to water availability at the biome-level based on AI, although spatial distribution of species-level drought sensitivity within and between ecosystems in a biome may vary significantly. We acknowledge that AI only captures a small portion of spatial variability in ecohydrological parameters, and there are many other factors that affect parameters that are often also correlated with AI.

5. Conclusions

We provide ecosystem-scale ecohydrological parameters for biomes with <60% woody vegetation consistent with observed probability distributions of satellite soil moisture and a parsimonious surface soil water balance. Inferred parameters integrate grid-scale plant water uptake dynamics from satellite observations and capture location-specific land cover and climate characteristics.

Our approach based on statistical properties of hydrologic and climatic variables overcomes some limitations of large-scale analyses, although satellite observations currently do not capture all plant water uptake (Text S1e). Our results characterize a diversity of drought-tolerant and drought-avoidant behaviors at a spatial scale beyond what has been possible using species-level traits. Further research is needed to relate ecosystem-scale plant water uptake strategies inferred from satellites with ground-truth observations.

Critical soil water potentials derived from a soil water balance may be more applicable to hydrological equations than those correlated with observable plant phenological change. Our results may improve commonly used empirical soil water-limitation functions compared to reference constants. A major challenge of this study is that the plant water uptake thresholds we infer are parameters models use to simplify the complex soil-plant-atmosphere continuum and are not quantities measured in the field. There is no direct method to validate our results against observations. Further research is needed to apply ecohydrological parameters inferred from satellite observations in hydrological and Earth system models and evaluate their performance.

Plant water uptake thresholds estimated in this study are consistent with surface soil moisture dynamics, and their relation to total biome evapotranspiration integrating the full rooting zone remains uncertain. It is uncertain to what extent dynamics of soil water evaporation affect our inferred thresholds because we are unable to partition soil moisture limitations on evaporation and transpiration. Further research is needed to determine whether plant water uptake thresholds inferred from surface soil moisture are different than those associated with deeper soil layers.

We provide a simple data-driven framework using global satellite data to diagnose the relation between plant water uptake and soil water balance that can enhance understanding of ecohydrological adaptation and resistance.

References

Akbar, R., Short Gianotti, D. J., Salvucci, G. D., & Entekhabi, D. (2019). Mapped Hydroclimatology of evapotranspiration and drainage runoff using SMAP brightness temperature observations and precipitation information. *Water Resources Research*, *55*(4), 3391–3413. https://doi.org/10.1029/2018WR024459

Anderegg, W. R. L., Klein, T., Bartlett, M., Sack, L., Pellegrini, A. F. A., Choat, B., & Jansen, S. (2016). Meta-analysis reveals that hydraulic traits explain cross-species patterns of drought-induced tree mortality across the globe. *Proceedings of the National Academy of Sciences*, *113*(18), 5024–5029. https://doi.org/10.1073/pnas.1525678113

Arsenault, K. R., Nearing, G. S., Wang, S., Yatheendradas, S., & Peters-Lidard, C. D. (2018). Parameter sensitivity of the Noah-MP land surface model with dynamic vegetation. *Journal of Hydrometeorology*, *19*(5), 815–830. https://doi.org/10.1175/jhm-d-17-0205.1

Baker, I. T., Prihodko, L., Denning, A. S., Goulden, M., Miller, S., & Da Rocha, H. R. (2008). Seasonal drought stress in the Amazon: Reconciling models and observations. *Journal of Geophysical Research*, *113*, G00B01. https://doi.org/10.1029/2007jg000644

Bassiouni, M. (2018). PIEP, version v1.0, Zenodo. https://doi.org/10.5281/zenodo.1257718

Bassiouni, M. (2020b). *Data_management_for_global_PIEP, Version v2*, Zenodo. https://doi.org/10.5281/zenodo.3235821

Bassiouni, M. (2020a). *Global dataset of ecohydrological parameters inferred from satellite observations, version V2.0*, Zenodo. https://doi.org/10.5281/zenodo.3605620

Bassiouni, M., Higgins, C. W., Still, C. J., & Good, S. P. (2018). Probabilistic inference of ecohydrological parameters using observations from point to satellite scales. *Hydrology and Earth System Sciences*, *22*(6), 3229–3243. https://doi.org/10.5194/hess-22-3229-2018

Bloom, A. A., & Williams, M. (2015). Constraining ecosystem carbon dynamics in a data-limited world: Integrating ecological "common sense" in a model–data fusion framework. *Biogeosciences*, *12*(5), 1299–1315. https://doi.org/10.5194/bg-12-1299-2015

Briggs, L. J., & Shantz, H. L. (1912). The wilting coefficient and its indirect determination. *Botanical Gazette*, *53*(1), 20–37. https://doi.org/10.1086/330708

Chan, S. K., Bindlish, R., O'Neill, P. E., et al. (2016). Assessment of the SMAP Passive Soil Moisture Product. *IEEE Transactions on Geoscience and Remote Sensing*, *54*(8), 4994–5007. https://doi.org/10.1109/tgrs.2016.2561938

Clark, D. B., Mercado, L. M., Sitch, S., Jones, C. D., Gedney, N., Best, M. J., et al. (2011). The Joint UK Land Environment Simulator (JULES), model description—Part 2: Carbon fluxes and vegetation dynamics. *Geoscientific Model Development*, *4*(3), 701–722. https://doi.org/10.5194/gmd-4-701-2011

Engelbrecht, B. M. J., Comita, L. S., Condit, R., Kursar, T. A., Tyree, M. T., Turner, B. L., & Hubbell, S. P. (2007). Drought sensitivity shapes species distribution patterns in tropical forests. *Nature*, *447*(7140), 80–82. https://doi.org/10.1038/nature05747

Entekhabi, D., Njoku, E. G., O'Neill, P. E., Kellogg, K. H., Crow, W. T., Edelstein, W. N., et al. (2010). The Soil Moisture Active passive (SMAP) Mission. *Proceedings of the IEEE*, *98*(5), 704–716. https://doi.org/10.1109/JPROC.2010.2043918

Evaristo, J., & McDonnell, J. J. (2017). Prevalence and magnitude of groundwater use by vegetation: A global stable isotope meta-analysis. *Scientific Reports*, *7*(1). https://doi.org/10.1038/srep44110, 1–12.

Fatichi, S., Pappas, C., & Ivanov, V. Y. (2016). Modeling plant-water interactions: An ecohydrological overview from the cell to the global scale: Modeling plant-water interactions. *Wiley Interdisciplinary Reviews Water*, *3*(3), 327–368. https://doi.org/10.1002/wat2.1125

Feddes, R. A., Kowalik, P., Kolinska-Malinka, K., & Zaradny, H. (1976). Simulation of field water uptake by plants using a soil water dependent root extraction function. *Journal of Hydrology*, *31*(1–2), 13–26. https://doi.org/10.1016/0022-1694(76)90017-2

Feldman, A. F., Short Gianotti, D. J., Konings, A. G., McColl, K. A., Akbar, R., Salvucci, G. D., & Entekhabi, D. (2018). Moisture pulse-reserve in the soil-plant continuum observed across biomes. *Nature Plants*, *4*(12), 1026–1033. https://doi.org/10.1038/s41477-018-0304-9

Fu, X., & Meinzer, F. C. (2019). Metrics and proxies for stringency of regulation of plant water status (iso/anisohydry): A global data set reveals coordination and trade-offs among water transport traits. *Tree Physiology*, *39*(1), 122–134. https://doi.org/10.1093/treephys/tpy087

Gelman, A., & Rubin, D. B. (1992). Inference from iterative simulation using multiple sequences. *Statistical Science*, *7*(4), 457–472. https://doi.org/10.1214/ss/1177011136

Good, S. P., Noone, D., & Bowen, G. (2015). Hydrologic connectivity constrains partitioning of global terrestrial water fluxes. *Science*, *349*(6244), 175–177. https://doi.org/10.1126/science.aaa5931

Hlavinka, P., Trnka, M., Balek, J., Semerádová, D., Hayes, M., Svoboda, M., et al. (2011). Development and evaluation of the SoilClim model for water balance and soil climate estimates. *Agricultural Water Management*, *98*(8), 1249–1261. https://doi.org/10.1016/j.agwat.2011.03.011

Jarvis, P. G., & Mcnaughton, K. G. (1986). Stomatal control of transpiration: scaling up from leaf to region. *Advances in ecological research*, *15*, 1–49. https://doi.org/10.1016/S0065-2504(08)60119-1

Kim, S. (2013). *Ancillary data report: Landcover classification (JPL D-53057)*. Pasadena, CA: Jet Propulsion.

Konings, A. G., & Gentine, P. (2017). Global variations in ecosystem-scale isohydricity. *Global Change Biology*, *23*(2), 891–905. https://doi.org/10.1111/gcb.13389

Laio, F., Porporato, A., Ridolfi, L., & Rodriguez-Iturbe, I. (2001). Plants in water-controlled ecosystems: Active role in hydrologic processes and response to water stress: II. Probabilistic soil moisture dynamics. *Advances in Water Resources*, *24*(7), 707–723. https://doi.org/10.1016/S0309-1708(01)00005-7

Li, X., Blackman, C. J., Choat, B., Duursma, R. A., Rymer, P. D., Medlyn, B. E., & Tissue, D. T. (2018). Tree hydraulic traits are coordinated and strongly linked to climate-of-origin across a rainfall gradient: Hydraulic traits coordination and link to climate. *Plant, Cell & Environment*, *41*(3), 646–660. https://doi.org/10.1111/pce.13129

Manfreda, S., Caylor, K. K., & Good, S. P. (2017). An ecohydrological framework to explain shifts in vegetation organization across climatological gradients: Vegetation pattern in dry environments. *Ecohydrology*, *10*(3), e1809. https://doi.org/10.1002/eco.1809

Manzoni, S., Vico, G., Katul, G., Palmroth, S., & Porporato, A. (2014). Optimal plant water-use strategies under stochastic rainfall. *Water Resources Research*, *50*, 5379–5394. https://doi.org/10.1002/2014WR015375

McColl, K. A., Wang, W., Peng, B., Akbar, R., Short Gianotti, D. J., Lu, H., et al. (2017). Global characterization of surface soil moisture drydowns. *Geophysical Research Letters*, *44*, 3682–3690. https://doi.org/10.1002/2017GL072819

Meinzer, F. C., Woodruff, D. R., Marias, D. E., Smith, D. D., McCulloh, K. A., Howard, A. R., & Magedman, A. L. (2016). Mapping 'hydroscapes' along the iso- to anisohydric continuum of stomatal regulation of plant water status. *Ecology Letters*, *19*(11), 1343–1352. https://doi.org/10.1111/ele.12670

Mencuccini, M., Manzoni, S., & Christoffersen, B. (2019). Modelling water fluxes in plants: From tissues to biosphere. *New Phytologist*, *222*(3), 1207–1222. https://doi.org/10.1111/nph.15681

Montzka, C., Herbst, M., Weihermüller, L., Verhoef, A., & Vereecken, H. (2017). A global data set of soil hydraulic properties and sub-grid variability of soil water retention and hydraulic conductivity curves. *Earth System Science Data*, *9*(2), 529–543. https://doi.org/10.5194/essd-9-529-2017

Müller, M. F., Dralle, D. N., & Thompson, S. E. (2014). Analytical model for flow duration curves in seasonally dry climates. *Water Resources Research*, *50*, 5510–5531. https://doi.org/10.1002/2014WR015301

Niu, G.-Y., Yang, Z.-L., Mitchell, K. E., Chen, F., Ek, M. B., Barlage, M., et al. (2011). The community Noah land surface model with multiparameterization options (Noah-MP): 1. Model description and evaluation with local-scale measurements. *Journal of Geophysical Research*, *116*, D12109. https://doi.org/10.1029/2010JD015139

Novick, K. A., Ficklin, D. L., Stoy, P. C., Williams, C. A., Bohrer, G., Oishi, A. C., et al. (2016). The increasing importance of atmospheric demand for ecosystem water and carbon fluxes. *Nature Climate Change*, *6*(11), 1023–1027. https://doi.org/10.1038/nclimate3114

O'Neill, P. E., Chan, S. K., Njoku, E. G., Jackson, T., & Bindlish, R. (2018). *SMAP L3 radiometer global daily 36 km EASE-Grid soil moisture, version 5*. [Indicate subset used]. Boulder, CO: NASA National Snow and Ice Data Center Distributed Active Archive Center. https://doi.org/10.5067/ZX7YX2Y2LHEBM.

Oleson, K., Lawrence, D. M., Bonan, G. B., Drewniak, B., Huang, M., Koven, C. D., et al. (2013). Technical description of version 4.5 of the Community Land Model (CLM) (No. NCAR/TN-503+STR), 434. https://doi.org/10.5065/D6RR1W7M

Or, D., Lehmann, P., Shahraeeni, E., & Shokri, N. (2013). Advances in soil evaporation physics—A review. *Vadose Zone Journal*, *12*(4), vzj2012.0163. https://doi.org/10.2136/vzj2012.0163

Oren, R., Sperry, J. S., Katul, G. G., Pataki, D. E., Ewers, B. E., Phillips, N., & Schäfer, K. V. R. (1999). Survey and synthesis of intra- and interspecific variation in stomatal sensitivity to vapour pressure deficit: Intra- and interspecific variation in stomatal sensitivity to vapour pressure deficit. *Plant, Cell & Environment*, *22*(12), 1515–1526. https://doi.org/10.1046/j.1365-3040.1999.00513.x

Pappas, C., Fatichi, S., & Burlando, P. (2016). Modeling terrestrial carbon and water dynamics across climatic gradients: Does plant trait diversity matter? *New Phytologist*, *209*(1), 137–151. https://doi.org/10.1111/nph.13590

Peng, L., Zeng, Z., Wei, Z., Chen, A., Wood, E. F., & Sheffield, J. (2019). Determinants of the ratio of actual to potential evapotranspiration. *Global Change Biology*, *25*(4), 1326–1343. https://doi.org/10.1111/gcb.14577

Porporato, A., Laio, F., Ridol, L., & Rodriguez-Iturbe, I. (2001). Plants in water-controlled ecosystems: Active role in hydrologic processes and response to water stress III. Vegetation water stress. *Advances in Water Resources*, *24*, 725–724. https://doi.org/10.1016/S0309-1708(01)00006-9

Powell, T. L., Galbraith, D. R., Christoffersen, B. O., Harper, A., Imbuzeiro, H. M. A., Rowland, L., et al. (2013). Confronting model predictions of carbon fluxes with measurements of Amazon forests subjected to experimental drought. *New Phytologist*, *200*(2), 350–365. https://doi.org/10.1111/nph.12390

Priestley, C. H. B., & Taylor, R. J. (1972). On the assessment of surface heat flux and evaporation using large-scale parameters. *Monthly Weather Review*, *100*(2), 81–92. https://doi.org/10.1175/1520-0493(1972)100<0081:OTAOSH>2.3.CO;2

Qiu, B., Xue, Y., Fisher, J. B., Guo, W., Berry, J. A., & Zhang, Y. (2018). Satellite chlorophyll fluorescence and soil moisture observations lead to advances in the predictive understanding of global terrestrial coupled carbon-water cycles. *Global Biogeochemical Cycles*, *32*, 360–375. https://doi.org/10.1002/2017GB005744

Reichle, R. H., De Lannoy, G. J., Koster, R. D., Crow, W. T., Kimball, J. S., & Liu, Q. (2018). *SMAP L4 radiometer global 3-hourly 9 km EASE-grid surface and root zone soil moisture geophysical data, version 4*. [Indicate subset used]. Boulder, CO: NASA National Snow and Ice Data Center Distributed Active Archive Center. https://doi.org/10.5067/KPJNN2GI1DQR

Richards, L. A., & Weaver, L. R. (1944). Moisture retention by some irrigated soils as related to soil moisture tension. *Journal of Agricultural Research*, *69*(6), 215–235.

Rodriguez-Iturbe, I., Gupta, V. K., & Waymire, E. (1984). Scale considerations in the modeling of temporal rainfall. *Water Resources Research*, *20*(11), 1611–1619. https://doi.org/10.1029/WR020i011p01611

Short Gianotti, D. J., Salvucci, G. D., Akbar, R., McColl, K. A., Cuenca, R., & Entekhabi, D. (2019). Landscape water storage and subsurface correlation from satellite surface soil moisture and precipitation observations. *Water Resources Research*, *55*(11), 9111–9132. https://doi.org/10.1029/2019WR025332

Skelton, R. P., West, A. G., & Dawson, T. E. (2015). Predicting plant vulnerability to drought in biodiverse regions using functional traits. *Proceedings of the National Academy of Sciences*, *112*(18), 5744–5749. https://doi.org/10.1073/pnas.1503376112

Steduto, P., Hsiao, T. C., Raes, D., & Fereres, E. (2009). AquaCrop—The FAO crop model to simulate yield response to water: I. concepts and underlying principles. *Agronomy Journal*, *101*(3), 426. https://doi.org/10.2134/agronj2008.0139s

Still, C. J., Berry, J. A., Collatz, G. J., & DeFries, R. S. (2003). Global distribution of C3 and C4 vegetation: Carbon cycle implications. *Global Biogeochemical Cycles*, *17*(1), 1006. https://doi.org/10.1029/2001gb001807

Stoy, P. C., El-Madany, T., Fisher, J. B., Gentine, P., Gerken, T., Good, S. P., et al. (2019). Reviews and syntheses: Turning the challenges of partitioning ecosystem evaporation and transpiration into opportunities. *Biogeosciences Discussions*, 1–47. https://doi.org/10.5194/bg-2019-85

Sultan, S. E. (2000). Phenotypic plasticity for plant development, function and life history. *Trends in Plant Science*, *5*(12), 537–542. https://doi.org/10.1016/S1360-1385(00)01797-0

Theil, H. (1992). A rank-invariant method of linear and polynomial regression analysis. In B. Raj & J. Koerts (Eds.), *Henri Theil's Contributions to Economics and Econometrics* (Vol. 23, pp. 345–381). Dordrecht, Netherlands: Springer. https://doi.org/10.1007/978-94-011-2546-8_20

Troch, P. A., Martinez, G. F., Pauwels, V. R. N., Durcik, M., Sivapalan, M., Harman, C., et al. (2009). Climate and vegetation water use efficiency at catchment scales. *Hydrological Processes*, *23*(16), 2409–2414. https://doi.org/10.1002/hyp.7358

Trugman, A. T., Medvigy, D., Mankin, J. S., & Anderegg, W. R. L. (2018). Soil moisture stress as a major driver of carbon cycle uncertainty. *Geophysical Research Letters*, *45*, 6495–6503. https://doi.org/10.1029/2018GL078131

Tyree, M. T. (2003). Plant hydraulics: The ascent of water. *Nature*, *423*(6943), 923. https://doi.org/10.1038/423923a

Westenbroek, S. M., Engott, J. A., Kelson, V. A., & Hunt, R. J. (2018). *SWB Version 2.0—A soil-water-balance code for estimating net infiltration and other water-budget components: U.S. Geological Survey Techniques and Methods* (book 6, chap. A59, 118 p.). https://doi.org/10.3133/tm6A59